Novel sulfonamide-β-lactam hybrids incorporating the piperazine moiety as potential iNOS inhibitors with promising antibacterial activity

Roghayeh Heiran, Aliasghar Jarrahpour, Elham Riazimontazer, Ahmad Gholami, Azza Troudi, Carole Di Giorgio, Jean Michel Brunel, Edward Turos

Novel sulfonamide-β-lactam hybrids incorporating the piperazine moiety as potential iNOS inhibitors with promising antibacterial activity

Roghayeh Heiran, *†,[a],[b] Aliasghar Jarrahpour, *†,[a] Elham Riazimontazer, *†,[c],[d],[e] Ahmad Gholami,[c],[d] Azza Troudi,[f] Carole Digiorgio,[g] Jean Michel Brunel [f] and Edward Turos [h]

[a] Dr. R. Heiran, Prof. A. Jarrahpour
Department of Chemistry, College of Sciences, Shiraz University, Shiraz, 71946-84795, Iran
E-mail: somaieheran@gmail.com, jarahpor@shirazu.ac.ir, aliasghar6683@yahoo.com
[b] Dr. R. Heiran
Department of Chemistry, Estahban Higher Education Center, Estahban 74519 44655, Iran
[c] Dr. E. Riazimontazer, Dr. A. Gholami
Biotechnology Research Center, Shiraz University of Medical Sciences, Shiraz, Iran
[d] Dr. E. Riazimontazer, Dr. A. Gholami
Pharmaceutical Sciences Research Center, Shiraz University of Medical Science, Shiraz, Iran
[e] Dr. E. Riazimontazer
Department of Medicinal Chemistry, School of Pharmacy, Shiraz University of Medical Sciences, Shiraz, Iran
[f] Dr. A. Troudi, Prof. J.M. Brunel
Aix Marseille Univ, INSERM, SSA, MCT, Marseille, France
[g] Dr. C. Digiorgio
Aix Marseille Université, CNRS, IRD, IMBE UMR 7263, Laboratoire de Mutagénèse Environnementale, 13385 Marseille, France
[h] Prof. E. Turos
Center for Molecular Diversity in Drug Design, Discovery, and Delivery, Department of Chemistry, CHE 205, 4202 East Fowler Avenue, University of South Florida, Tampa, Florida, 33620 USA

† These authors contributed equally to this work
* Corresponding authors

Supporting information for this article is given via a link at the end of the document.

Abstract: Several novel monocyclic *β*-lactams bearing the piperazine moiety have been synthesized and evaluated for their biological activities. *β*-Lactams **4b** and **4h** exhibited 31 and 27 anti-inflammatory ratios, respectively, which are as well as the well-known dexamethasone corticosteroid with a 32 anti-inflammatory ratio. The two most active compounds **4b** and **4h** showed IC_{50} values more than 200 µM against the HepG2 cell line, in comparison with doxorubicin (IC_{50} < 1 µM), indicated biocompatibility and nontoxic behavior. **4d**, **4j**, **4k** and **4l**, were active against *S. aureus* and *E. coli* and have broad spectrum property. The tested compounds were subjected to *in silico* prediction of pharmacokinetics properties (ADMET) to assess the potential *in vivo* effectiveness. Molecular docking study confirmed that the active inhibitors **4b** and **4h** are well fitted in the iNOS active site. This data suggests that **4b** and **4h** could potentially serve as effective iNOS inhibitors a represent promising lead compounds for treating inflammatory disorders.

Introduction

Nitric oxide (NO) has been found to have a crucial role as a powerful cellular signaling molecule. NO is responsible for different physiological functions in mammals such as vasodilation, smoot muscle relaxation, neurotransmission, and immune response. Formation of NO as a free radical in cells is orchestrated by the enzymatic oxidation of L-arginine (L-Arg) to L-citrulline by a family of enzymes called nitric oxide synthases (NOSs). There are three isoforms of NOS, including neuronal NOS (nNOS) and endothelial NOS (eNOS) that are constitutively expressed, while the third one is inducible and is thus termed inducible nitric oxide synthase (iNOS) [1]. nNOS is the isoform first found in the nervous system, while eNOS is the isoform first found in vascular endothelial cells. iNOS is not the constant present mediator in cells and is only expressed once the cell is induced or stimulated [2]. Cell stimulation arises typically by proinflammatory cytokines and/or bacterial lipopolysaccharide (LPS) to produce iNOS, which generates micromolar amount of NO [3–5]. This significant amount of NO is critical for the inflammatory response and the innate immune system to help defend against invading pathogens. Inappropriately high NO concentration due to the overexpression or dysregulation of iNOS arised a variety of human diseases, including septic shock, cardiac dysfunction, pain diabetes, and cancers [4]. Therefore, controlling its detrimental effects and maintaining its proper physiological functions depends on regulation of its production. Because of the important role of iNOS, the selective inhabitation of its enzymatic activity is an effective therapeutic strategy [6]. Several *in vitro* methods have been reported to measure iNOS activity during the use of iNOS inhibitors. One assay is a cell-based system, where a macrophage cell line (such as RAW 264.7 effective) [7,8] is stimulated to express iNOS by action of added cytokines. In this case, the way to monitor NO production is, for example, via the addition of Griess reagent to cell lysates, which detects nitrite production.

Sulfonamides are a broad class of biologically active compounds that are widely used in different number of therapeutic areas. A variety of sulfonamides possess anti-

inflammatory [9–11], anticancer [10], antidiabetic [12,13], anti-HIV [14], antifungal [15], antibacterial and antioxidant [11] activities. On the other hand, piperazine is one of the most important pharmacophores in medicinal chemistry [16], with widespread antidepressant [17], anticancer [18], antipsychotic [19], anti-HIV [20], and antimicrobial [21,22] properties. This six-membered ring is present in some cardiovascular agents like Prazosin [23], Lidoflazin [24], and Urapidil [25]. Sulfonamides bearing the piperazine moiety have been reported to have antidiabetic [26], anti-HIV [27], anticancer [28], antimicrobial [29,30], and anti-acetylcholinesterase [31] activities.

β-Lactams are another highly unique class of heterocyclic compounds possessing diverse biological applications as anti-HIV [32], antimalarial [33], antimicrobial [34–37], antioxidant [38,39], anti-inflammation [40,41], and anticancer activities [40,42,43]. *β*-Lactam is the core component of naturally compounds such as penicillins, cephalosporins, clavams, carbapenems and the monocyclic *β*-lactams, which are produced by a wide range of organisms [44,45]. The monobactam nucleus provides an individual scaffold to study the effect of structural modification at the N-1, C3 and C4 positions of the *β*-lactam (2-azetidinone) ring on biological activity [46]. Some *β*-lactam derivatives bearing a piperazine moiety **(Figure 1)** have displayed promising antimicrobial **(I, II)** [47,48], antitumor **(III)** [49], antiurease and antioxidant **(IV)** [50] activities as well as tryptase inhibition **(V- VIII)** [51–54].

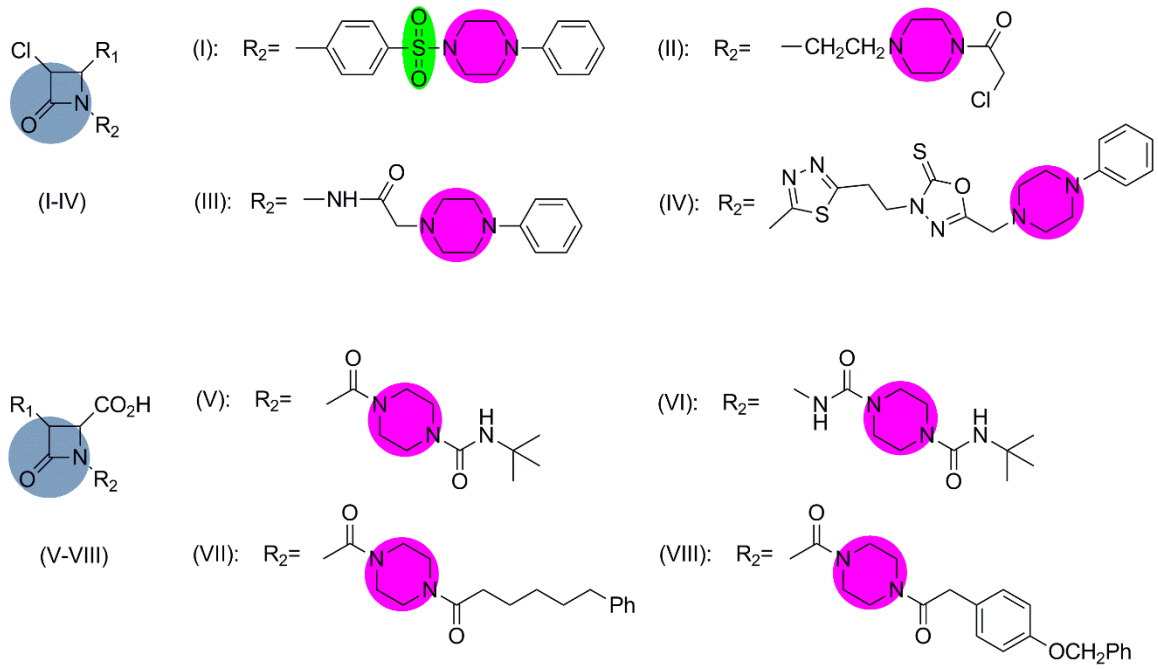

Figure 1. Some derivatives of *β*-lactams **(I-VIII)** bearing the piperazine moiety.

Here, as a part of our ongoing efforts devoted to the design of bioactive heterocycles [40,41,55–58], we synthesized a series of sulfonamide-*β*-lactam analogues possessing a pendant piperazine moiety, and evaluated their anti-inflammatory activities by the cell-based assay, cytotoxicity, and antibacterial activities. In order to gather additional insight about the potential interactions and optimal binding mode of the active derivatives in the binding site of iNOS, computational molecular dicking analyses were performed. Finally, all compounds were investigated for drug-likeness criteria and they were subjected to *in silico* techniques to predict pharmacokinetic properties including absorption, distribution, metabolism, excretion, and toxicity (ADMET).

Results and Discussion

Chemistry

The synthesis of *β*-lactams bearing the piperazine moiety were performed by using a classical Staudinger imine-ketene cycloaddition reaction, as outlined in **Scheme 1**. Thus, 1-(2-aminoethyl)-piperazine **(1)** was treated with different aromatic aldehydes in solvent-free condition at room temperature to provide the expected imines **(3).** Treatment of the imines with the desired ketenes, prepared *in situ* from substituted acetic acid and *p*-toluenesulfonyl chloride in CH_2Cl_2 at room temperature in the presence of triethylamine, led to the formation of the new *β*-lactams **4a-l (Table 1)**.

The formation of *β*-lactam derivatives **4a-l** was evidenced by the appearance of infrared absorption bands at 1735-1758 and 1320-1396 cm^{-1} due to the *β*-lactam C=O and S=O in the IR spectrum, respectively. In the ^{1}H-NMR spectra, the observed coupling constants of the vicinal H-3 and H-4 protons of the *β*-lactam ring confirmed the *cis* stereochemistry of these new *β*-lactam compounds. As an example, the IR spectrum of **4b** showed characteristic absorption peaks at 1751 and 1350 cm^{-1}

for the *β*-lactam carbonyl group and SO_2, respectively. The ^{1}H-NMR spectrum of **4b** displayed aliphatic chain, piperazine ring, methyl and methoxy protons as broad multiplet absorptions at 2.43-2.45, 2.95, 3.05-3.16 and 3.55-3.65 ppm, respectively. The *β*-lactam H-3 and H-4 protons appeared as two doublets at 5.41 (J = 4.4 Hz) and 5.06 (J = 4.4 Hz), respectively, that confirmed the *cis* stereochemistry for this product. Aromatic protons appeared as a doublet at 6.66 (J = 7.8 Hz) and multiplets ranging from 6.77 to 7.77 ppm. In addition, the ^{13}C-NMR spectrum of **4b** displayed a *β*-lactam carbonyl signal at 166.3 ppm. Aliphatic chain and piperazine ring carbons appeared at 37.3, 45.9, 51.8 and 54.9 ppm, and methyl carbon was observed at 21.6 ppm. Moreover, the C-4 and C-3 carbons of the *β*-lactam ring appeared at 62.9 and 82.3 ppm, respectively, whereas the aromatic carbons appear from 114.4 to 156.9 ppm.

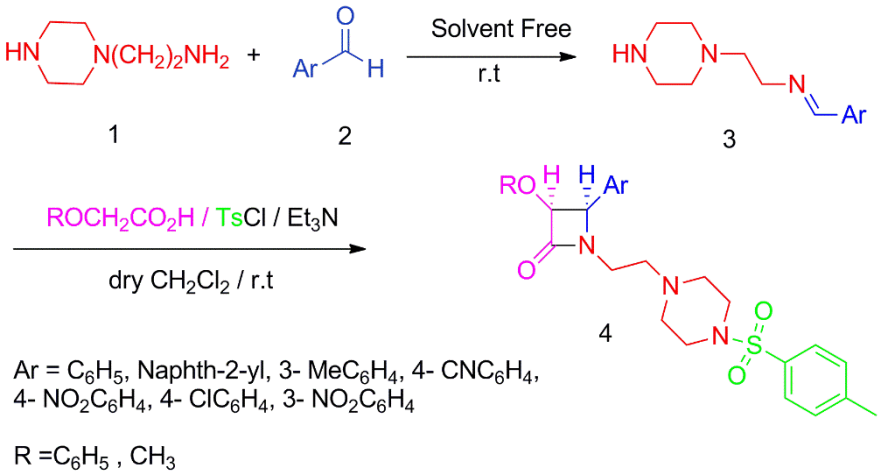

Ar = C_6H_5, Naphth-2-yl, 3- MeC_6H_4, 4- CNC_6H_4, 4- $NO_2C_6H_4$, 4- ClC_6H_4, 3- $NO_2C_6H_4$

R =C_6H_5 , CH_3

Scheme 1. Some derivatives of *β*-lactams **(I-VIII)** bearing the piperazine moiety.

Table 1. Structures of monocyclic β-lactams **4a-l**

Entry	Name	R	Ar	Isolated Yield (%)
1	**4a**	Ph	Ph	34
2	**4b**	Ph	Naphthyl	53
3	**4c**	Ph	3-MeC_6H_4	49
4	**4d**	Ph	4-ClC_6H_4	68
5	**4e**	Ph	4-CNC_6H_4	61
6	**4f**	Ph	4-$NO_2C_6H_4$	59
7	**4g**	CH_3	Ph	28
8	**4h**	CH_3	Naphthyl	47
9	**4i**	CH_3	3-MeC_6H_4	43
10	**4j**	CH_3	4-ClC_6H_4	44
11	**4k**	CH_3	4-CNC_6H_4	50
12	**4l**	CH_3	3-$NO_2C_6H_4$	51

Structure-activity relationship of the compounds 4a-l

Results concerning the anti-inflammatory activity of the different β-lactam derivatives are reported in **Table 2**. We noted that six compounds presented good anti-inflammatory ratio values varying from 10 to 31. Two derivatives, 4b and 4h, with a therapeutic ratio of 31 and 27, respectively, appeared as active as the well-known dexamethasone [40] (therapeutic ratio of 32), a corticosteroid medication used in the treatment of rheumatic problems and skin diseases. Interestingly, an important analogy between the structures 4b and 4h is the presence of a naphthyl ring moiety, which enhances lipophilicity; log P value as can be seen in **Table 4**. The presence of a phenoxy group at the C3 position, and electron-rich aryl substituents (3-MeC6H4 and naphthyl) at the C4 position of β-lactam ring in **4b** and **4c**, likewise showed more potent anti-inflammatory activity than having a methoxy group at C3 and an electron-donating substituent at C4 as for comparative analogues **4h** and **4i**.

The finding that having a naphthyl moiety at the C4 position in both compounds **4b** and **4h** provides for the most potent anti-inflammatory activity may implicate stronger hydrophobic interactions and more spatial occupation of the enzyme active site. The binding modes of **4b** and **4h** compared to dexamethasone within the human inducible nitric oxide synthase active site are illustrated in **Figure 4** and **5**. The presence of the C4 naphthyl moiety on the β-lactam ring had a positive effect on

the anti-inflammatory, antibacterial and cytotoxic activity and the calculated minimum Gibbs binding energy as well. Furthermore, amongst the compounds having an electron withdrawing moiety (e.g. Cl and CN) on the C4 phenyl ring of the β-lactam, we observed that replacing the C3 phenoxy group **(4d-e)** with the methoxy group **(4j-k)** decreased the anti-inflammatory activity.

Table 2. Anti-inflammatory activity of derivatives **4a-4l**

Name	$IC_{50\text{-NO release}}$ (μM)	$IC_{50\text{-cell viability}}$ (μM)	Anti-Inflammatory ratio	IC_{50} (μM) ± Std. HepG2
4a	112.28 ± 5.47	251.28 ± 6.24	2	55.57 ± 5.19
4b	7.90 ± 1.24	247.40 ± 8.56	31	>200
4c	11.18 ± 1.08	249.27 ± 10.36	22	>200
4d	32.05 ± 2.08	319.32 ± 15.32	10	39.06 ± 4.68
4e	23.01 ± 1.83	246.69 ± 9.47	11	49.64 ± 5.27
4f	>500	>500	-[a]	51.26 ± 0.91
4g	70.33 ± 3.14	322.87 ± 8.15	5	55.38 ± 3.19
4h	9.27± 1.52	246.14 ± 10.47	27	>200
4i	34.01 ± 2.89	220.77 ± 9.31	6	135.54 ± 17.32
4j	3.21 ± 0.95	16.14 ± 0.98	5	21.01 ± 3.02
4k	22.47 ± 1.99	192.58 ± 9.56	9	15.42 ± 2.17
4l	23.93 ± 1.58	222.88 ± 13.24	10	27.10 ± 5.20
Dexamethasone	5.02 ± 1.34	159.2 ± 26.35	32	-[a]
Doxorubicin				<1

[a] Not determined due to insolubility in the media

Cytotoxicity evaluation

For evaluation of cell viability and detection of synthesized sulfonamide-*β*-lactam hybrids toxicity the MTT assay was applied based on mitochondrial activity and metabolism of an immortalized HepG2 cell line. This assay as a colorimetric method reduced MTT, a yellow tetrazole, to purple formazan in living cells and the absorbance of the colored solution was measured by a spectrophotometer at a certain wavelength. In present assay, the viability percent of HepG2 cells was assigned after treatment with synthesized sulfonamide-*β*-lactam hybrids in different concentrations (1–200 μM) (**Figure 2**). As it could be concluded from **Figure 2** and **Table 2**, the IC_{50} value represent the metabolic activity affected by all tested sulfonamide-*β*-lactam with a concentration-dependent manner. **Figure 2** indicated that increasing concentration of all compounds from 1 to 200 μM leads to cytotoxicity enhancement. IC_{50} values between 135 μM and 15 μM could be observed for most of the compounds, higher than the anticancer agent doxorubicin (IC_{50} < 1 μM). As a result, our findings propose that these sulfonamide-*β*-lactam hybrids might be safe, nontoxic and biocompatible to the HepG2 cell line. The potent compounds **4b** and **4h** with IC_{50} values more than 200 μM indicated better biocompatibility and nontoxic behavior in comparison to doxorubicin (IC_{50} < 1 μM).

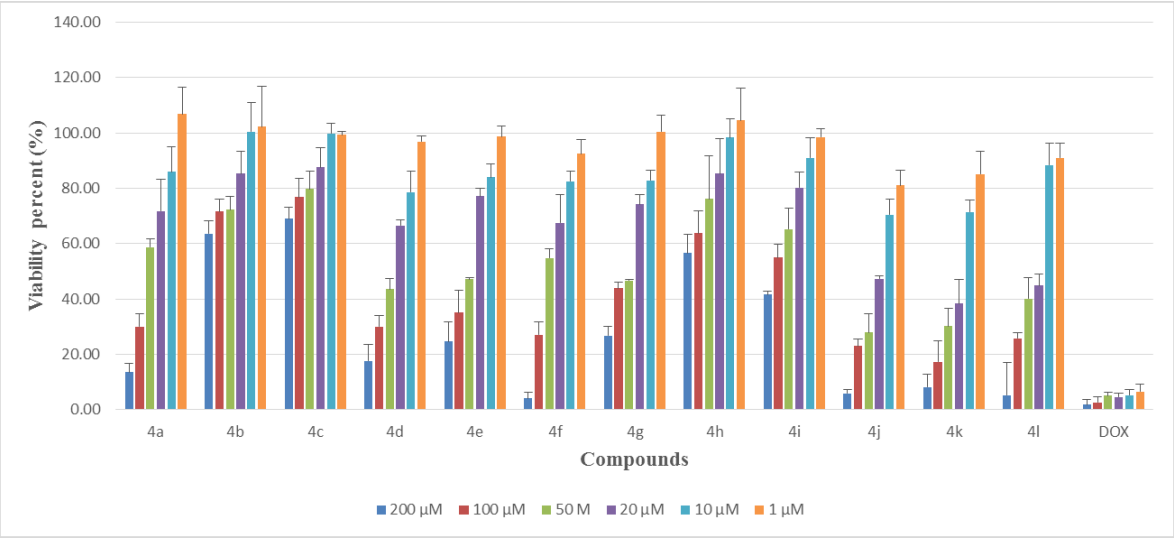

Figure 2. Viability percentage of the HepG2 cells treated with synthesized sulfonamide-*β*-lactam hybrids in different concentrations 1- 200 µM.

Antimicrobial activity

The *in* vitro antibacterial susceptibility of the synthesized sulfonamide-β-lactam hybrids was screened against two bacterial strains from both gram positive and gram negative groups *S. aureus* and *E. coli* by microdilution method indicated by minimum inhibitory concentration (MIC). As it could be seen in **Figure 3** the compounds reveal a dose dependent bacterial growth inhibition. The MIC values of the tested bacterial strains have been shown in **Table 3**. The MIC values for **4b** and **4h** were 32 µM and more than 32 µM against both bacterial strains in comparison with ampicillin (MIC = 1), therefore they did not exhibit significant antibacterial activity. In addition, **4d**, **4j**, **4k** and **4l** exhibited stronger antibacterial activity with MIC lower than 4 µM against both bacterial strains. Amongst them **4j** with 4-Cl substituent on the phenyl ring is the most active one as well as ampicillin as the standard agent with MIC<1 µM. Therefore, they could be broad spectrum compounds amongst all the synthesized sulfonamide-*β*-lactam hybrids. These results represent that an important requirement for the antibacterial activity might be an optimal lipophilicity. The introduction of naphthyl moiety into the structures reduced the antibacterial activity due to the higher lipophilicity.

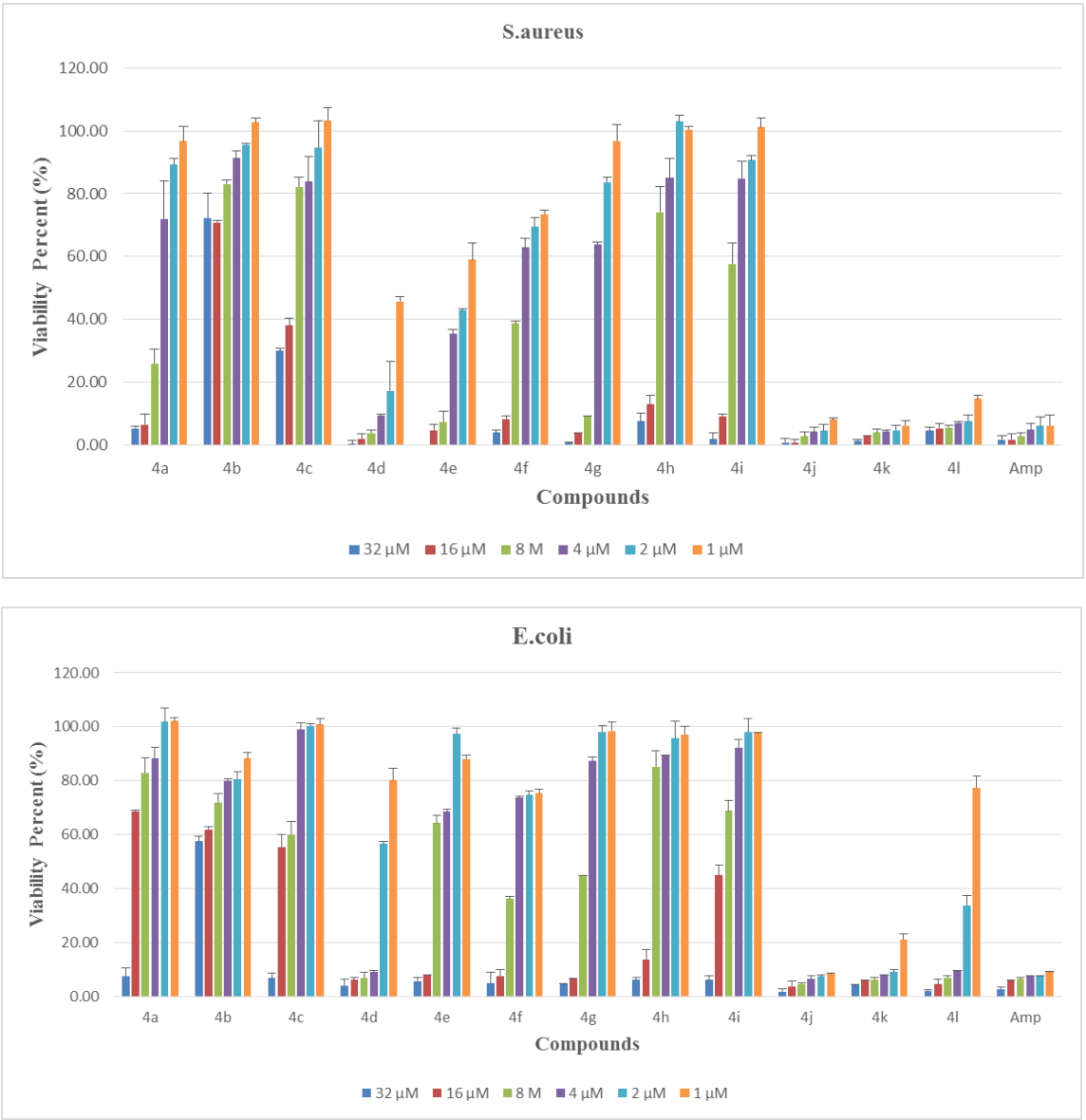

Figure 3. Viability percentage of *E. coli* and *S. aureus* in tested concentrations of tested synthesized sulfonamide β-lactam hybrids.

Table 3. Antimicrobial Activities of synthesized sulfonamide-β-lactam hybrids against bacteria (μM).

Code	MIC (μM)	
	S. aureus	E. coli
4a	16	32
4b	>32	>32
4c	>32	32
4d	4	4
4e	8	16
4f	16	16
4g	8	16
4h	32	32
4i	16	32
4j	1	1
4k	1	2
4l	2	4
Ampiciline	1	1

In order to satisfy drug-like characteristics for evaluating good absorption or permeation, compounds must have some physio-chemical properties. They are included: molecular weight (MW) ≤ 500; calculated partition coefficient (CLog P) ≤ 5; the number of rotatable bonds (NRB) ≤ 10; the number of hydrogen bond donors (NHBD) ≤ 5; the number of hydrogen bond acceptors (NHBA) ≤ 10; and polar surface area no greater than 140 Å2 [59].

All compounds were screened on the base of Lipinski and Veber rules to investigate the physiochemical properties of the compounds using the Swiss ADME online server (**Table 4**). The data revealed that there is no more than one violation of the Lipinski's criteria in the rule of five and in the Veber rule. All compounds have log P values lower than 5.0, indicating that the compounds are not very lipophilic. This reflects a good agreement with their hydrogen bond properties. The compounds all have a total polar surface area (TPSA) value and a rotatable bond number lower than 140 and 10, respectively. It could be concluded that **4b** and **4h**, both being highly potent compounds, have good absorption or permeation features, and are predicted to have good oral bioavailability.

Computational study

In silico prediction of physicochemical properties

Table 4. *In silico* physicochemical parameters of **4a-l** possessing iNOS inhibitory activity.

Code	LogP [a]	HBA [b]	HBD [c]	TPSA [d]	nRB [e]	MW [f]	Number of Lipinski violations	Druglikeness	
								Lipinski	Veber
4a	3.30	6	0	78.54	8	505.63	1	Yes	Yes
4b	4.12	6	0	78.54	8	555.69	1	Yes	Yes
4c	3.65	6	0	78.54	8	519.66	1	Yes	Yes
4d	3.85	6	0	78.54	8	540.07	1	Yes	Yes
4e	3.08	7	0	102.33	8	530.64	1	Yes	Yes
4f	2.52	8	0	124.36	9	550.63	1	Yes	Yes
4g	2.15	6	0	78.54	7	443.56	0	Yes	Yes
4h	3.04	6	0	78.54	7	493.62	0	Yes	Yes
4i	2.46	6	0	78.54	7	457.59	0	Yes	Yes
4j	2.64	6	0	78.54	7	478.00	0	Yes	Yes
4k	1.90	7	0	102.33	7	468.57	0	Yes	Yes
4l	1.38	8	0	124.36	8	488.56	0	Yes	Yes
Dexamethasone	2.15	6	3	94.83	2	392.46	0	Yes	Yes

[a] Logarithm of partition coefficient between n-octanol and water (Log P).

[b] Number of hydrogen bond acceptors (HBA).

[c] Number of hydrogen bond donors (HBD).

[d] Topological polar surface area (TPSA).

[e] Number of rotatable bonds (nRB).

[f] Molecular weight (MW).

In silico prediction of pharmacokinetic (ADMET) properties

Pharmacokinetic (ADMET) properties of **4b** and **4h,** the most potent iNOS inhibitors in this study, were calculated using the web-based application pkCSM in order to determine the perfectness of fit of the compounds in the protein binding pocket [60]. The clinical enzyme inhibitor dexamethasone was used for comparison. The results are summarized in **Table 5**. Compounds **4a** and **4b** show high intestinal absorption (predicted value > 95), which indicates that they could more effectively be absorbed in the body. Moreover, the high Caco-2 permeability value (predicted value > 0.90) indicates that the derivatives could readily penetrate biological membranes such as intestinal mucosa. The compounds are predicted to have good solubility in water at 25ºC (log S = -6.5 to 0.5). The most potent iNOS inhibitors, **4b** and **4h**, are predicted to have skin permeability (log Kp = -2.73 and -2.74 cm h^{-1}) comparable to dexamethasone (log Kp = -3.93 cm h^{-1}).

The P-glycoprotein is an ATP-binding cassette (ABC) transporter. As a biological barrier, the P-glycoprotein actively exports toxins and xenobiotics out of cells. The predictor determines that the compounds are likely the substrates of Pgp and the inhibitors of Pgp I and II. Relatively low blood–brain barrier permeation is observed for them (logBB < 0), which means they are poorly distributed to the brain, and less likely to cause neurotoxicity. They are also unlikely to penetrate the CNS (logPS < -2.5). Cytochrome P450 is an important detoxification and metabolic enzyme involved in the formation and breakdown of various molecules and chemicals within the cell, mainly found in the liver. The results are shown in **Table 5**. Organic Cation Transporter 2 (OCT2) is a renal uptake transporter that mediates the deposition and renal clearance of organic cations. The potent compounds **4b** and **4h** are substrates of OCT2 in comparison to dexamethasone. They are likely to have total clearance as a combination of hepatic clearance and renal clearance, as is the case for dexamethasone.

Table 5. *In silico ADME profiling of the most potent compounds with iNOS inhibitory activity and dexamethasone.*

Property	Model Name	Unit	4b	4h	Dexa
			Predicted Value		
	Water solubility	(log mol/L)	**-4.64**	**-5.338**	**-3.465**
	Caco2 permeability	(log Papp in 10-6 cm/s)	**1.178**	**1.227**	**0.918**
Absorption	**Intestinal absorption (human)**	(% Absorbed)	**95.173**	**95.387**	**77.925**
	Skin Permeability	(log Kp)	**-2.735**	**-2.741**	**-3.928**
	P-glycoprotein substrate	Categorical	**Yes**	**Yes**	**Yes**
	P-glycoprotein I inhibitor	Categorical	**Yes**	**Yes**	**No**
	P-glycoprotein II inhibitor	Categorical	**Yes**	**Yes**	**No**
	VDss (human)	(log L/kg)	**-0.395**	**0.342**	**0.165**
Distribution	**Fraction unbound (human)**	(Fu)	**0.155**	**0.009**	**0.291**
	BBB permeability	(log BB)	**-0.102**	**-0.127**	**-0.923**
	CNS permeability	(log PS)	**-2.274**	**-2.571**	**-3.279**
Metabolism	**CYP2D6 substrate**	Categorical	**No**	**No**	**No**
	CYP3A4 substrate	Categorical	**Yes**	**Yes**	**No**
	CYP1A2 inhibitor	Categorical	**No**	**No**	**No**
	CYP2C19 inhibitor	Categorical	**Yes**	**Yes**	**No**
	CYP2C9 inhibitor	Categorical	**Yes**	**Yes**	**No**

	CYP2D6 inhibitor	Categorical	**No**	**No**	**No**
	CYP3A4 inhibitor	Categorical	**Yes**	**Yes**	**No**
	Total Clearance	(log ml/min/kg)	**0.320**	**0.504**	**0.662**
Excretion	**Renal OCT2 substrate**	Categorical	**Yes**	**Yes**	**No**

In this study the protox-II, a freely available webserver, was used for toxicity verification of the potent compounds, **4b** and **4h** [61,62]. Toxicity classes in ProTox server are defined according to the globally harmonized system of classification of labeling of chemicals (GHS), where classes I and II are fatal, class III is toxic, class IV is harmful, and class V may be harmful while class VI is non-toxic in nature. These two compounds, **4b** and **4h**, are inactive for nuclear receptor signalling and stress response pathways including aryl hydrocarbon receptor (AhR). They are also inactive for hepatotoxicity, carcinogenicity, immunotoxicity, mutagenicity and cytotoxicity which is consistant with MTT assay results. The predicted LD_{50} for both compounds **4b** and **4h** are 1000 mg/kg. These compounds also are not active for the heat shock response (HSE). In comparison, dexamethasone is active for immunotoxicity and some nuclear receptor signaling pathways such as androgen receptor (AR) and androgen receptor ligand binding domain (AR-LBD). The predicted toxicity of active compounds **4b** and **4h** is listed in **Table 6.** In the toxicity prediction, both were lying in toxicity class IV; meanwhile, dexamethasone was in toxicity class V.

Table 6. *In silico predicted toxicity of active compounds with iNOS inhibitory activity and dexamethasone.*

Comp.	**4b**	**4h**	**Dexa**
Endpoint			
Predicted LD50	1000 mg/kg (67.38%)	1000 mg/kg (67.38%)	3000 mg/kg (100%)
(prediction accuracy %)			
Hepatotoxicity (probability)	Inactive (0.61)	Inactive (0.61)	Inactive (0.99)
Carcinogenicity (probability)	Inactive (0.64)	Inactive (0.64)	Inactive (0.72)
Immunotoxicity (probability)	Inactive (0.96)	Inactive (0.93)	Active (0.99)
Mutagenicity (probability)	Inactive (0.69)	Inactive (0.68)	Inactive (0.69)
Cytotoxicity (probability)	Inactive (0.71)	Inactive (0.71)	Inactive (0.72)
AhR (probability)	Inactive (0.92)	Inactive (0.93)	Inactive (1.00)
AR (probability)	Inactive (0.88)	Inactive (0.86)	Active (1.00)
AR-LBD (probability)	Inactive (0.88)	Inactive (0.88)	Active (1.00)
Heat shock factor response element (HSE) (probability)	Inactive (0.95)	Inactive (0.95)	Inactive (1.00)
Predicted toxicity class	IV	IV	V

Docking study with inducible nitric oxide synthase

In an effort to further validate the experimental results and to ascertain the binding pose of the most potent compounds **4b** and **4h** in the active site of human inducible nitric oxide synthase, ligand-protein visualization was performed by means of Auto Dock Vina (1.1.2). There is variety of X-ray crystal structures of human inducible nitric oxide synthase in Protein Data Bank (PDB), which is complexed with different ligands. Therefore, six 3D X-ray crystal structures of nitric oxide synthase were retrieved from Protein Data Bank (PDB). 3E7G (RMSD=0.50 Å) had the best docking validation score amongst 1NSI, 2NSI, 3E7G, 3EJ8 and 4NOS that had been picked out based on optimal self-docking criteria of RMSD < 2 Å (**Table 7**).

Cross-docking of the synthesized compounds was performed after self-docking survey. After termination of the cross-docking simulation, the binding energies of each ligand along with the residues involved in the interaction were reported for visualization and analysis. The results of cross-docking studies for all five PDB codes are shown in **Table 7**. As it can be seen from the results of binding energies and interactions for five PDB codes, compounds **4b** and **4h** exhibited the best docking scores and also they have the most potent *in vitro* iNOS inhibitory activity, with IC_{50} = 7.90 and 9.27 µM, respectively, in comparison with dexamethasone with IC_{50} = 5.02. The molecular docking results for visualization of protein and compounds 4b and 4h represented well fitted coordination with active site pocket. Interactions of **4b** and **4h** with the protein active site are illustrated in **Figure 4** for five PDB codes.

As shown in **Figure 4**, the naphthyl group of **4b** created π-π stacking interaction with the indole ring of Trp463 (3E7G) and cation-π interaction with the positively charged nitrogen of Arg388 (1NSI, 3EJ8), and Arg381(2NSI, 3E7G and 4NOS). The phenoxy moiety of **4b** interacted with the indole ring of Trp463 (1NSI, 2NSI, 3EJ8 and 4NOS) by a π-π stacking interaction and also showed cation-π interaction with Arg381 (1NSI, 2NSI, 3EJ8 and 4NOS). The positively charged nitrogens of Asn354 and Gln263 made a hydrogen bond with the oxygen atom of the sulfonamide moiety and a cation-π interaction with the nitrogen atom of Arg266 (1NSI and 3E7G).

On the other hand, the naphthyl group of **4h** adopted an orientation through π-π stacking against the indole ring of Trp463 (1NSI, 3E7G and 4NOS), and formed cation-π interactions with Arg381 (1NSI, 3E7G and 4NOS) and Arg388 (2NSI). Also, Arg266 (1NSI) and Gln263 (3E7G) adopted hydrogen bonds through the oxygen atom of the sulfonamide moiety and Gln263 is the residue responsible for hydrogen bonding with the amide oxygen atom of the *β*-lactam (3EJ8) (**Figure 4**).

Dexamethasone was likewise computationally docked into the receptor and demonstrated a similar binding pose to the *β*-lactams, forming hydrogen bonds and hydrophobic interactions with the main residues in the active site pocket. The superimposition of most active compound **4b** with dexamethasone in the enzyme binding site of iNOS is depicted in **Figure 5**. Docking results of residues involved in the interactions of **4b**, **4h** and dexamethazone in different x-ray crystal structures has been shown in **Table 8.**

The above docking study implied that **4b** and **4h** were in good agreement either by the calculated Gibbs binding energy or *in vitro* evaluation results. Our results of the present molecular docking study supported the binding of these compounds to the active site of iNOS. These results could be consistent with our molecular design for iNOS inhibition.

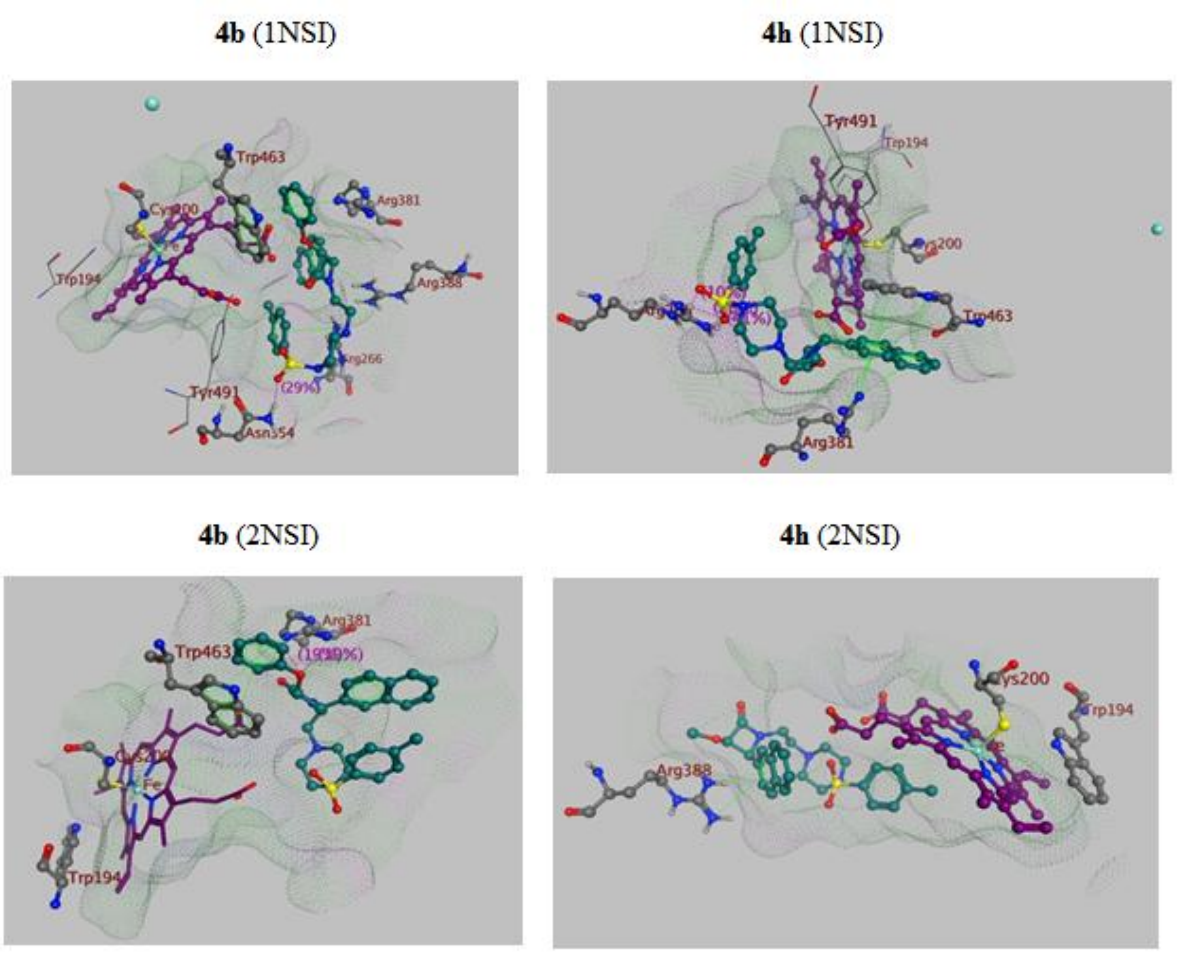

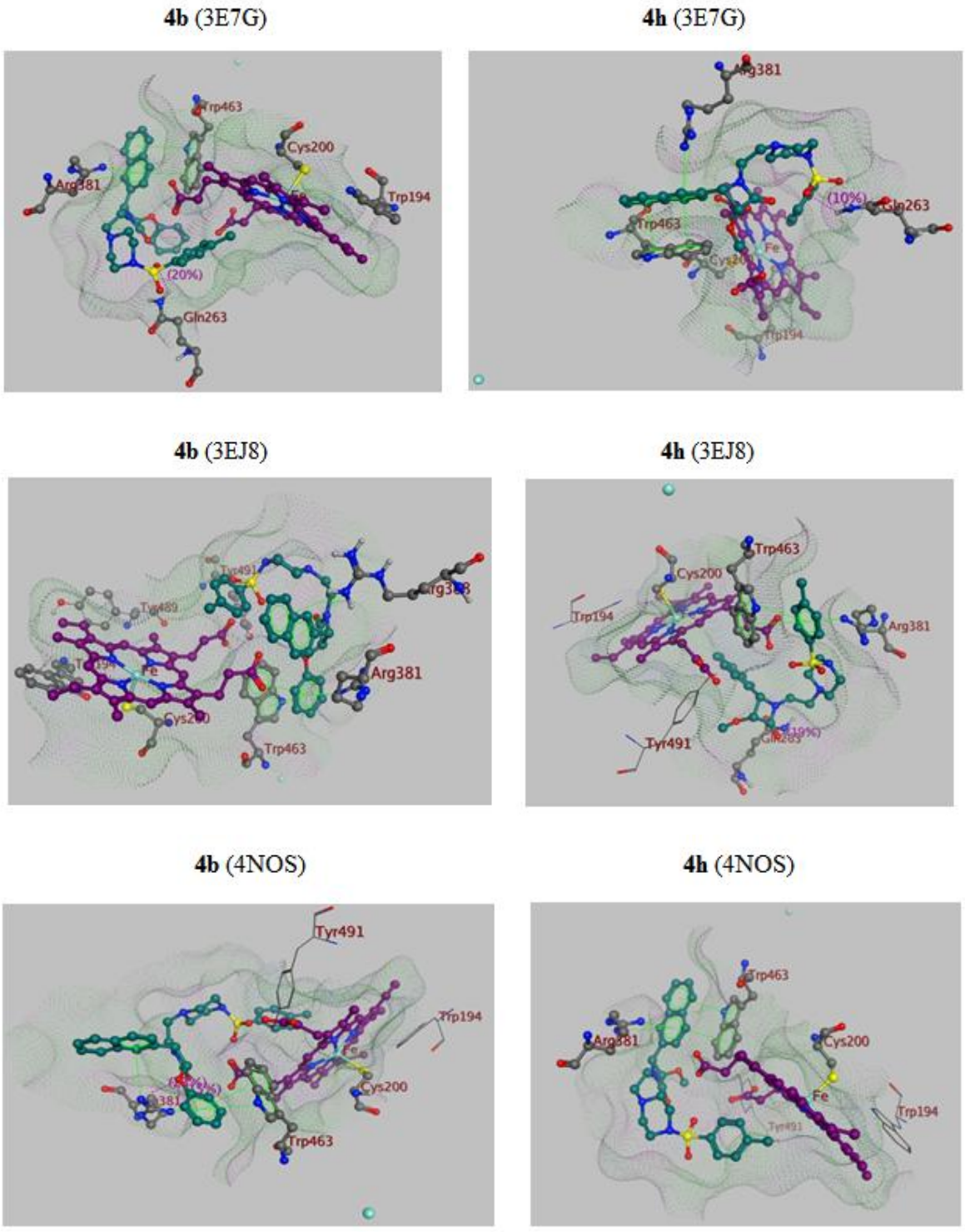

Figure 4. The best pose of the most active compounds **4b** and **4h** with different x-ray crystal structures (PDB code: 1NSI, 2NSI, 3E7G, 3EJ8 and 4NOS) in the active site of human inducible nitric oxide synthase; and the residues of the active site involved in ligand binding.

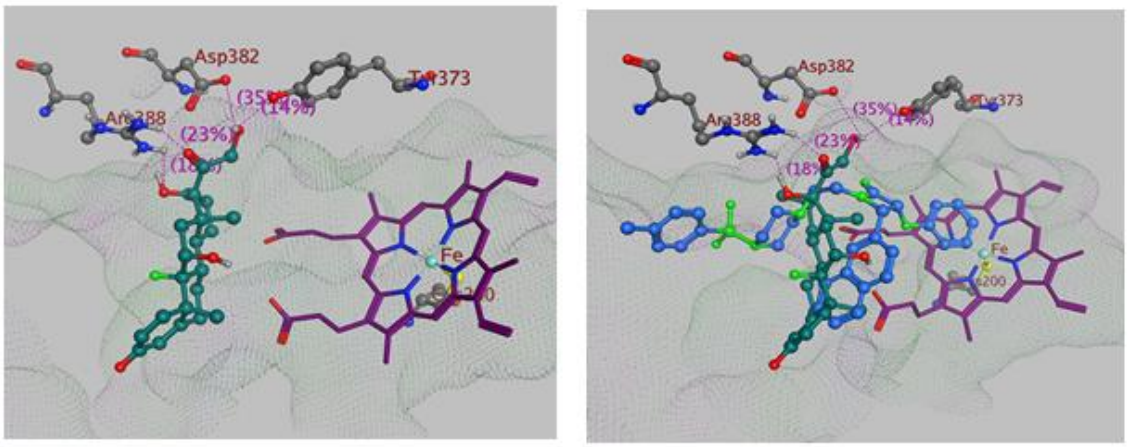

Figure 5. The best pose of dexamethasone with x-ray crystal structures (PDB code: 2NSI) in the active site of iNOS; and the residues of the active site involved in ligand binding (left). Superimposition of **4b** (blue) and dexamethasone (green) within the enzyme binding site (right).

Table 7. *RMSD values and binding energies of all derivatives and dexamethasone as a standard compound with different x-ray crystal structures (PDB code: 1NSI, 2NSI, 3E7G, 3EJ8 and 4NOS).*

	PDB Code	1nsi	2nsi	3e7g	3ej8	4cx7	4nos
	RMSD	0.6	0.8	0.5	0.8	4.7	0.6
Compounds: Binding Energy (Kcal.mol^{-1})	4a	-9.4	-10.1	-10.2	-9.7	-11.2	-10.8
	4b	-10.7	-11.4	-11	-10.9	-12.4	-11.7
	4c	-9	-10.7	-10.6	-10.4	-11.5	-11.2
	4d	-9.7	-10.7	-10.4	-10.3	-11.4	-10.8
	4e	-9.3	-11	-10.6	-10.5	-11.1	-11.1
	4f	-9.3	-10.9	-10.1	-10.4	-10.9	-10.9
	4g	-8.4	-8.7	-8.9	-8.9	-9.6	-9.4
	4h	-10	-10.4	-10.4	-10.4	-10.4	-11.3
	4i	-8.9	-9.4	-9.2	-9.7	-9.8	-10
	4j	-8.6	-9	-9.3	-9.3	-9.7	-9.6
	4k	-8.9	-9.4	-9.8	-9.5	-9.5	-10
	4l	-8.7	-9.4	-9.4	-9.7	-9.8	-9.8
	4m	-9.3	-9.2	-9.5	-9.4	-9.4	-9.3
	Dexamethasone	-7.7	-8.5	-8	-7.8	-8.5	-8.3

Table 8. *Docking results of residues involved in the interactions of **4b**, **4h** and dexamethazone in different x-ray crystal structures (PDB codes: 1NSI, 2NSI, 3E7G, 3EJ8 and 4NOS).*

PDB Code	Comp.	Hydrogen bond	Hydrophobic interaction	π-π	π-Cation	Metal Complexes
1NSI	4b	Asn354	Ala262,Tyr373, Glu377, Arg381, Arg700	Trp463	Arg38, Arg38, Arg266	Cys200 (Fe) Cys110, Cys 115(Zn)
	4h	Arg266, Arg388	Ala262, Val352, Ile462	Trp463	Arg381	Cys200 (Fe) Cys110, Cys 115 (Zn)
2NSI	4b	Arg381	Ala282, Gln387	Trp463	Arg381	Cys200 (Fe)
	4h	Arg388	Pro350, Val352,Glu377, Arg381		Arg388	Cys200 (Fe)

3E7G	4b	Gln263, Arg388	Pro350, Val352, Ile462, Trp463, Tyr491	Trp463	Arg381	Cys200 (Fe)
						Cys110, Cys 115(Zn)
	4h	Gln263, Arg388	Pro350, Val352, Ilu462	Trp463	Arg381	Cys200 (Fe)
						Cys110, Cys 115(Zn)
3EJ8	4b	Arg266, Arg381	Gln263, Pro350, Val352, Tyr373, Glu377, Arg381	Trp463	Arg381	Cys200 (Fe)
						Cys110, Cys 115(Zn)
	4h	Gln263, Arg381	Pro350, Val352, Trp463		Arg381	Cys200 (Fe)
						Cys110, Cys 115(Zn)
4NOS	4b	Gln263, Arg381	Pro350,	Trp463		Cys200 (Fe)
			Val352, Gln387, Arg388			Cys110, Cys 115(Zn)
		Gln263, Arg388	Pro350, Val352, Ilu462	Trp463	Arg381	Cys200 (Fe)
						Cys110, Cys 115(Zn)
Dexamethasone		Arg381, Arg388, Asp382, Gln263, Arg266, Val284, Glu285, Tyr373, Glu377,	Trp463, Tyr491, Arg388, Gln387, Arg381, Ala282			Cys200 (Fe)

Conclusion

A series of new *β*-lactam rings bearing a piperazine moiety as an appended side chain were synthesized based on the natural monocyclic *β*-lactam scaffolds via a [2+2] ketene-imine cycloaddition reaction. The *β*-lactams were evaluated for their inhibitory effect on inducible nitric oxide synthase (iNOS). Compounds **4b** and **4h**, containing a naphthyl moiety at the C4 position of the *β*-lactam ring, were the most potent derivatives against iNOS with an IC_{50} value of 7.90±1.24 μM and 9.27±1.52 μM and anti-inflammatory ratio 31 and 27, respectively, which was comparable to that of dexamethasone (5.02±1.34 μM) and anti-inflammatory ratio 32. In addition, they were evaluated for potential *in vitro* antibacterial activity. **4d**, **4j**, **4k** and **4l,** showed good antibacterial activity against either the Gram-negatives *E. coli* or the Gram-positive *S. aureus* in comparison with ampicillin as a standard. Therefore, they could be considering as broad spectrum compounds. All compounds showed low cytotoxicity towards HepG2 cell line at or above the bacterial minimum inhibitory concentration. In the molecular docking results, the lower Gibbs binding energies of the most potent compounds **4b** and **4h** were consistent with the *in vitro* evaluation results. Derivatives were subjected to *in silico* prediction of physicochemical and pharmacokinetic properties in order to determine the perfectness of the compounds. Based on the obtained data we consider the tested compounds to have good physicochemical properties indicated that the compounds are compliant with the Lipinski and Veber rules. ADMET prediction for the two most active compounds **4b** and **4h** indicated that they have good solubility, high intestinal absorption, good biological membrane penetration and low blood–brain barrier permeation. They have also good skin permeability comparable to dexamethasone. From the results of *in silico* study, we conclude that **4b** and **4h** may be considered as potent iNOS inhibitors with low toxicity. However, they both were lying in toxicity class IV based on the toxicity prediction. Conclusively, these compounds may lead to the discovery of promising modified structures as well as a novel candidate for inflammatory diseases with antibacterial activity. Further work with the aim of improving the structure of the most active compounds are now under current investigation in our laboratory.

Experimental Section

Materials and methods

All the reagents were purchased from Merck, Acros, and Fluka companies and used without any purification. Methylene

chloride (CH_2Cl_2) and Triethylamine (Et_3N) were dried by distillation over CaH_2 and then stored over 4 A° molecular sieves. Thin layer chromatography (TLC) was carried out on silica gel 254 analytical sheets obtained from Fluka and visualized by UV lamp. Purification of products was achieved by silica gel column chromatography on Merck Kiesel gel (230–270 mesh). ^{1}H-NMR and ^{13}C-NMR spectra were recorded on a Bruker avance DPX spectrometer (250 MHz for ^{1}H and62.9 MHz for ^{13}C) in $CDCl_3$ using tetramethylsilane (TMS) as internal standard. Chemical shifts (σ) are given in part per million (ppm), and the coupling constants (*J*) are expressed in Hertz. Infrared spectroscopy analysis was recorded on a Shimadzu FT-IR 8300 spectrophotometer and the sample and KBr were pressed to form a tablet. The mass spectra were taken on Shimadzu GC–MS QP 1000 EX instrument. Elemental analyses were run on a Thermo Finnigan Flash EA-1112series, and the melting points were determined in open capillaries with a Buchi 510 melting point apparatus.

General Procedure for the Synthesis of Monocyclic β-lactams (4a-l)

A mixture of 2-(piperazin-1-yl) ethanamine **(1)** (10.00 mmol) and different aromatic aldehydes **(2)** (10.00 mmol) was mixed without solvent for 5-15 minutes. The crude Schiff bases **(3)** were used for the next step without any further purification. Then, to a stirred solution of N-[(1)-arylmethylidene]-2-piperazin-1-ylethanamine (**3**) (4.00 mmol) in dry CH_2Cl_2 (20 mL), *p*-toluenesulfonyl chloride (10.00 mmol) and trimethylamine (18.00 mmol) were added, and the mixture was stirred for about 30 minutes at room temperature. The acetic acid derivative (6.00 mmol) was then added to the mixture and the reaction was continued for 12 hours at room temperature. After the reaction was completed (TLC monitoring), the mixture was washed with aqueous HCl (1 N), saturated $NaHCO_3$ solution, and NaCl solution, dried and the solvent was evaporated to afford the crude *β*-lactams **4a-l**. The crude products were purified either by recrystallization from EtOAc or column chromatography (2:1 petroleum ether/EtOAc).

Characterization of new synthesized products

*3-Phenoxy-4-phenyl-1-(2-(4-tosylpiperazin-1-yl)ethyl) azetidin-2-one **(4a)***

White solid recrystallized from EtOAc (yield 34%). mp: 177-179 °C. IR (KBr, cm^{-1}): 1396 (S=O), 1758 (CO, *β*-lactam). ^{1}H NMR ($CDCl_3$) δ 2.45 (CH_3 and CH_2, br, 9H), 2.93 (CH_2, br, 4H), 3.04-3.14 (CH_2, m, 1H), 3.52-3.62 (CH_2, m, 1H), 4.88 (H-4, d, *J* = 4.4 Hz, 1H), 5.34 (H-3, d, *J* = 4.4 Hz, 1H), 6.65 (ArH, d, *J* = 7.9 Hz, 2H), 6.82-7.26 (ArH, m, 8H), 7.34 (ArH, d, *J* = 8.2 Hz, 2H), 7.62 (ArH, d, *J* = 8.0 Hz, 2H). ^{13}C NMR ($CDCl_3$) δ 21.6 (CH_3), 37.2, 45.9, 51.9, 54.9 (CH_2), 62.7 (C-4), 82.1 (C-3), 115.5, 121.9, 127.8, 128.1, 128.5, 128.6, 129.1, 129.7, 132.5, 133.2, 143.7, 156.8 (aromatic carbons), 166.1 (CO, *β*-lactam). MS m/z = 505 [M^+]. Anal. calcd. for $C_{28}H_{31}N_3O_4S$: C, 66.51; H, 6.18; N, 8.31; S, 6.34. Found: C, 66.63; H, 6.25; N, 8.27; S, 6.21.

*4-(Naphthalen-2-yl)-3-phenoxy-1-(2-(4-tosylpiperazin-1-yl) ethyl)azetidin-2-one **(4b)***

White solid recrystallized from EtOAc (yield 53%). mp: 199-201 °C. IR (KBr, cm^{-1}): 1350 (S=O), 1751 (CO, *β*-lactam). ^{1}H NMR ($CDCl_3$) δ 2.43-2.45 (CH_3 and CH_2, br, 9H,), 2.95 (CH_2, br, 4H), 3.05-3.16 (CH_2, m, 1H), 3.55-3.65 (CH_2, m, 1H), 5.06 (H-4, d, *J* = 4.4 Hz, 1H), 5.41 (H-3, d, *J* = 4.4 Hz, 1H), 6.66 (ArH, d, *J* = 7.8 Hz, 2H), 6.77-7.77 (ArH, m, 14H). ^{13}C NMR ($CDCl_3$) δ 21.6 (CH_3), 37.2, 45.9, 51.9, 54.9 (CH_2), 62.9 (C-4), 82.3 (C-3), 114.4, 115.5, 122.0, 125.7, 126.3, 126.4, 127.7, 127.8, 128.2, 128.9, 129.1, 129.8, 130.9, 132.6, 132.8, 133.3, 143.7, 156.9 (aromatic carbons), 166.3 (CO, *β*-lactam). MS m/z = 555 [M^+]. Anal. calcd. for $C_{32}H_{33}N_3O_4S$: C, 69.17; H, 5.99; N, 7.56; S, 5.77. Found: C, 69.29; H, 6.14; N, 7.59; S, 5.70.

*3-Phenoxy-4-m-tolyl-1-(2-(4-tosylpiperazin-1-yl)ethyl) azetidin-2-one **(4c)***

White solid recrystallized from EtOAc (yield 49%). mp: 156-158 °C. IR (KBr, cm^{-1}): 1372 (S=O), 1751 (CO, *β*-lactam). ^{1}H NMR ($CDCl_3$) δ 2.24(CH_3, s, 3H), 2.45 (CH_3 and CH_2, br, 9H), 2.96 (CH_2, br, 4H), 3.01-3.12 (CH_2, m, 1H), 3.52-3.63 (CH_2, m, 1H), 4.84 (H-4, d, *J* = 4.4 Hz, 1H), 5.32 (H-3, d, *J* = 4.4 Hz, 1H), 6.67 (ArH, d, *J* = 7.7 Hz, 2H), 6.83-7.14 (ArH, m, 7H), 7.33 (ArH, d, *J* = 8.0 Hz, 2H), 7.62 (ArH, d, *J* = 8.2 Hz, 2H). ^{13}C NMR ($CDCl_3$) δ 21.3, 21.5 (CH_3), 37.1, 45.9, 51.9, 54.9 (CH_2), 62.6 (C-4), 82.1 (C-3), 115.6, 121.9, 125.6, 127.8, 128.0, 129.1, 129.1, 129.4, 129.8, 132.5, 132.7, 137.7, 144.0, 156.9 (aromatic carbons), 163.2 (CO, *β*-lactam). MS m/z = 519 [M^+]. Anal. calcd. for $C_{29}H_{33}N_3O_4S$: C, 67.03; H, 6.40; N, 8.09; S, 6.17. Found: C, 67.21; H, 6.49; N, 8.03; S, 6.09.

*4-(4-Chlorophenyl)-3-phenoxy-1-(2-(4-tosylpiperazin-1-yl) ethyl)azetidin-2-one **(4d)***

White solid recrystallized from EtOAc (yield 68%). mp: 191-193 °C. IR (KBr, cm^{-1}): 1320 (S=O), 1751 (CO, *β*-lactam). ^{1}H NMR ($CDCl_3$) δ 2.41-2.45 (CH_3 and CH_2, br, 9H), 2.92-2.93 (CH_2, br, 4H), 3.02-3.13(CH_2, m, 1H), 3.49-3.59(CH_2, m, 1H), 4.87 (H-4, d, *J* = 4.4 Hz, 1H), 5.33 (H-3, d, *J* = 4.4 Hz, 1H), 6.65 (ArH, d, *J* = 8.4 Hz, 2H), 6.84-7.19 (ArH, m, 7H), 7.34 (ArH, d, *J* = 8.2 Hz, 2H), 7.61 (ArH, d, *J* = 8.2 Hz, 2H). ^{13}C NMR ($CDCl_3$) δ 21.6 (CH_3), 37.2, 45.9, 51.9, 54.9 (CH_2), 62.1 (C-4), 81.9 (C-3), 115.4, 122.2, 127.8, 128.3, 129.2, 129.7, 129.8, 132.1, 132.4, 134.4, 143.8, 156.6 (aromatic carbons), 165.9 (CO, *β*-lactam). MS m/z = 539 [M^+]. Anal. calcd. for $C_{28}H_{30}ClN_3O_4S$: C, 62.27; H, 5.60; N, 7.78; S, 5.94. Found: C, 62.35; H, 5.79; N, 7.74; S, 5.89.

*4-(4-Oxo-3-phenoxy-1-(2-(4-tosylpiperazin-1-yl)ethyl) azetidin-2-yl)benzonitrile **(4e)***

White solid purified by column chromatography (eluent 2:1 petroleum ether /EtOAc) (yield 61%). mp: 201-203 °C. IR (KBr, cm^{-1}): 1342 (S=O), 1751 (CO, *β*-lactam), 2229 (CN). ^{1}H NMR ($CDCl_3$) δ 2.41-2.47 (CH_2, br, 6H), 2.47 (CH_3, s, 3H), 2.89 (CH_2, br, 4H), 3.06-3.17 (CH_2, m, 1H), 3.52-3.63 (CH_2, m, 1H), 4.95 (H-4, d, *J* = 4.5 Hz, 1H), 5.39 (H-3, d, *J* = 4.5 Hz, 1H), 6.63 (ArH, d, *J* = 8.6 Hz, 2H), 6.85-7.43 (ArH, m, 9H), 7.61 (ArH, d, *J* = 8.1 Hz, 2H). ^{13}C NMR ($CDCl_3$) δ 21.6 (CH_3), 37.5, 45.8, 51.9, 54.9

(CH_2), 62.1 (C-4), 82.1 (C-3), 112.3, 115.3, 118.3, 122.3, 127.8, 128.8, 129.0, 129.3, 129.8, 130.9, 132.4, 143.9, 156.3 (aromatic carbons), 165.7 (CO, *β*-lactam). MS m/z = 531 [M^+]. Anal. calcd. for $C_{29}H_{30}N_4O_4S$: C, 65.64; H, 5.70; N, 10.56; S, 6.04. Found: C, 65.80; H, 5.82; N, 10.50; S, 5.96.

4-(4-Nitrophenyl)-3-phenoxy-1-(2-(4-tosylpiperazin-1-yl)ethyl) azetidin-2-one ***(4f)***

White solid recrystallized from EtOAc (yield 59%). mp: 175-177 °C. IR (KBr, cm^{-1}): 1350, 1519, (NO_2), 1388 (S=O), 1751 (CO, *β*-lactam). ^{1}H NMR ($CDCl_3$) δ 2.45-2.47 (CH_3 and CH_2, br, 9H), 2.95 (CH_2, br, 4H), 3.08-3.16 (CH_2, m, 1H), 3.55-3.63 (CH_2, m, 1H), 5.01 (H-4, d, *J* = 4.5 Hz, 1H), 5.41 (H-3, d, *J* = 4.5 Hz, 1H), 6.64 (ArH, d, *J* = 7.7 Hz, 2H), 6.85-7.43 (ArH, m, 7H), 7.61 (ArH, d, *J* = 8.3 Hz, 2H), 7.99 (ArH, d, *J* = 8.8 Hz, 2H). ^{13}C NMR ($CDCl_3$) δ 21.6 (CH_3), 37.5, 45.9, 51.9, 54.9 (CH_2), 61.9 (C-4), 82.2 (C-3), 115.3, 122.4, 123.2, 127.8, 129.2, 129.4, 129.8, 130.9, 132.4, 143.9, 147.9, 156.3 (aromatic carbons), 165.6 (CO, *β*-lactam). MS m/z = 550 [M^+]. Anal. calcd. for $C_{28}H_{30}N_4O_6S$: C, 61.08; H, 5.49; N, 10.18; S, 5.82. Found: C, 61.00; H, 5.68; N, 10.15; S, 5.75.

3-Methoxy-4-phenyl-1-(2-(4-tosylpiperazin-1-yl)ethyl)azetidin-2-one ***(4g)***

White solid recrystallized from EtOAc (yield 28%) mp: 153-155 °C. IR (KBr, cm^{-1}): 1357 (S=O), 1751 (CO, *β*-lactam). ^{1}H NMR ($CDCl_3$) δ 2.37-2.42 (CH_2, br, 6H), 2.47 (CH_3, s, 3H), 2.92 (CH_2, br, 4H), 3.03-3.09 (CH_2, m, 1H), 3.05 (OCH_3, s, 3H), 3.43-3.54 (CH_2, m, 1H), 4.60 (H-4, d, *J* = 4.4 Hz, 1H), 4.71 (H-3, d, *J* = 4.4 Hz, 1H), 7.26-7.30 (ArH, m, 5H,), 7.30 (ArH, d, *J* = 7.9 Hz, 2H), 7.61 (ArH, d, *J* = 8.3 Hz, 2H). ^{13}C NMR ($CDCl_3$) δ 21.6 (CH_3), 36.9, 45.9, 51.8, 54.9 (CH_2), 58.0 (OCH_3), 62.3 (C-4), 85.7 (C-3), 127.8, 128.2, 128.2, 128.5, 129.7, 132.5, 133.9, 143.7 (aromatic carbons), 167.2 (CO, *β*-lactam). MS m/z = 443 [M^+]. Anal. calcd. for $C_{23}H_{29}N_3O_4S$: C, 62.28; H, 6.59; N, 9.47; S, 7.23. Found: C, 62.39; H, 6.75; N, 9.43; S, 7.15.

3-Methoxy-4-(naphthalen-2-yl)-1-(2-(4-tosylpiperazin-1-yl) ethyl)azetidin-2-one ***(4h)***

White solid recrystallized from EtOAc (yield 47%). mp: 121-123 °C. IR (KBr, cm^{-1}): 1350 (S=O), 1735 (CO, β-lactam). ^{1}H NMR ($CDCl_3$) δ 2.31 (CH_2, br, 6H), 2.37 (CH_3, s, 3H), 2.85 (CH_2, br, 4H), 2.92 (OMe, s, 3H), 2.94-3.03 (CH_2, m, 1H), 3.39-3.47 (CH_2, m, 1H), 4.59 (H-4, d, J = 4.1 Hz, 1H), 4.79 (H-3, d, J = 4.1 Hz, 1H), 7.26 (ArH, d, J = 7.7 Hz, 2H), 7.32-7.72 (ArH, m, 9H). ^{13}C NMR ($CDCl_3$) δ 21.6 (CH_3), 37.1, 45.9, 51.8, 54.9 (CH_2), 58.1 (OCH_3), 62.5 (C-4), 85.9 (C-3), 125.6, 126.3, 126.4, 127.8, 127.9, 129.8, 131.6, 132.5, 132.9, 133.4, 143.7 (aromatic carbons), 167.3 (CO, β-lactam). MS m/z = 493 [M^+]. Anal. calcd. for $C_{27}H_{31}N_3O_4S$: C, 65.70; H, 6.33; N, 8.51; S, 6.50. Found: C, 65.84; H, 6.49; N, 8.63; S, 6.42.

3-Methoxy-4-m-tolyl-1-(2-(4-tosylpiperazin-1-yl)ethyl) azetidin-2-one ***(4i)***

White solid recrystallized from EtOAc (yield 43%). mp: 161-163 °C. IR (KBr, cm^{-1}): 1350 (S=O), 1735 (CO, *β*-lactam). ^{1}H NMR ($CDCl_3$) δ 2.31 (s, 3H, CH_3), 2.37-2.43 (m, 6H, CH_2), 2.46 (s, 3H, CH_3), 2.92 (br, 4H, CH_2), 3.00-3.06 (m, 1H, CH_2), 3.06 (s, 3H, OCH_3), 3.45-3.55 (m, 1H, CH_2), 4.59 (d, *J* = 4.4 Hz, 1H, H-4), 4.66 (d, *J* = 4.4 Hz, 1H, H-3), 7.03-7.20 (ArH, m, 4H), 7.34 (ArH, d, *J* = 8.0 Hz, 2H), 7.61 (ArH, d, *J* = 8.3 Hz, 2H). ^{13}C NMR ($CDCl_3$) δ 21.4, 21.5 (CH_3), 36.9, 45.9, 51.9, 54.9 (CH_2), 58.1 (OCH_3), 62.3 (C-4), 85.6 (C-3), 125.4, 127.8, 128.1, 128.8, 129.3, 129.7, 130.1, 133.8, 137.9, 143.7 (aromatic carbons), 167.3 (CO, *β*-lactam). MS m/z = 457 [M^+]. Anal. calcd. for $C_{24}H_{31}N_3O_4S$: C, 63.00; H, 6.83; N, 9.18; S, 7.01. Found: C, 63.24; H, 6.99; N, 9.13; S, 6.85.

4-(4-Chlorophenyl)-3-methoxy-1-(2-(4-tosylpiperazin-1-yl) ethyl)azetidin-2-one ***(4j)***

White solid purified by column chromatography (eluent 2:1 petroleum ether /EtOAc) (yield 44%). mp: 131-133 °C. IR (KBr, cm^{-1}): 1342 (S=O), 1735 (CO, *β*-lactam). ^{1}H NMR ($CDCl_3$) δ 2.37-2.44 (CH_2, m, 6H), 2.47 (CH_3, s, 3H), 2.90 (CH_2, br, 4H), 2.96-3.08 (CH_2, m, 1H), 3.05 (OCH_3, s, 3H), 3.41-3.52 (CH_2, m, 1H), 4.59 (H-4, d, *J* = 4.4 Hz, 1H), 4.68 (H-3, d, *J* = 4.4 Hz, 1H), 7.17-7.23 (ArH, m, 4H), 7.36 (ArH, d, *J* = 8.3 Hz, 2H), 7.61 (ArH, d, *J* = 8.3 Hz, 2H). ^{13}C NMR ($CDCl_3$) δ 21.6 (CH_3), 37.0, 45.9, 51.8, 54.9 (CH_2), 58.2 (OCH_3), 61.7 (C-4), 85.7 (C-3), 127.8, 128.5, 129.6, 129.8, 132.4, 132.6, 134.4, 143.8 (aromatic carbons), 167.1 (CO, *β*-lactam). MS m/z = 478 [M^+]. Anal. calcd. for $C_{23}H_{28}ClN_3O_4S$: C, 57.79; H, 5.90; N, 8.79; S, 6.71. Found: C, 57.90; H, 6.14; N, 8.73; S, 6.65.

4-(3-Methoxy-4-oxo-1-(2-(4-tosylpiperazin-1-yl)ethyl) azetidin-2-yl)benzonitrile ***(4k)***

White solid purified by column chromatography (eluent 2:1 petroleum ether /EtOAc) (yield 50%). mp: 119-121 °C. IR (KBr, cm^{-1}): 1334 (S=O), 1735 (CO, *β*-lactam). ^{1}H NMR ($CDCl_3$) δ 2.41 (CH_2, br, 6H), 2.49 (CH_3, s, 3H), 2.87 (CH_2, br, 4H), 3.00-3.11 (CH_2, m, 1H), 3.06 (OCH_3, s, 3H), 3.44-3.55 (CH_2, m, 1H), 4.64 (H-4, d, *J* = 4.5 Hz, 1H), 4.77 (H-3, d, *J* = 4.5 Hz, 1H), 7.37-7.42 (ArH, m, 4H), 7.50 (ArH, d, *J* = 8.2 Hz, 2H), 7.61 (ArH, d, *J* = 8.2 Hz, 2H). ^{13}C NMR ($CDCl_3$) δ 21.5 (CH_3), 37.3, 45.8, 51.8, 54.8 (CH_2), 58.3 (OCH_3), 61.9 (C-4), 85.9 (C-3), 112.2, 118.4, 127.8, 128.9, 129.8, 131.9, 132.3, 140.1, 143.9 (aromatic carbons), 166.9 (CO, *β*-lactam). MS m/z = 470 [M^+]. Anal. calcd. for $C_{24}H_{28}N_4O_4S$: C, 61.52; H, 6.02; N, 11.96; S, 6.84. Found: C, 61.60; H, 6.19; N, 11.93; S, 6.59.

3-Methoxy-4-(3-nitrophenyl)-1-(2-(4-tosylpiperazin-1-yl)ethyl) azetidin-2-one ***(4l)***

White solid recrystallized from EtOAc (yield 51%). mp: 139-141 °C. IR (KBr, cm^{-1}): 1350, 1535, (NO_2), 1342 (S=O), 1751 (CO, *β*-lactam). ^{1}H NMR ($CDCl_3$) δ 2.41 (CH_2, br, 6H), 2.48 (CH_3, s, 3H), 2.90 (CH_2, br, 4H), 3.07-3.17 (CH_2, m, 1H), 3.08 (OCH_3, s, 3H), 3.44-3.54 (CH_2, m, 1H), 4.66 (H-4, d, *J* = 4.4 Hz, 1H), 4.84 (H-3, d, *J* = 4.4 Hz, 1H), 7.36 (ArH, d, *J* = 8.3 Hz, 2H), 7.44-8.15 (ArH, m, 6H). ^{13}C NMR ($CDCl_3$) δ 21.6 (CH_3), 37.4, 45.9, 51.9, 54.9 (CH_2), 58.4 (OCH_3), 61.6 (C-4), 85.8 (C-3), 123.2, 123.5, 127.7, 129.2, 129.8, 132.4, 134.2, 136.9, 143.9, 148.1 (aromatic carbons), 167.0 (CO, *β*-lactam). MS m/z = 489 [M^+]. Anal. calcd. for $C_{23}H_{28}N_4O_6S$: C, 56.54; H, 5.78; N, 11.47; S, 6.56. Found: C, 56.60; H, 5.89; N, 11.43; S, 6.39.

In vitro anti-inflammatory activity[63]

Principle of the assay

The *in vitro* anti-inflammatory assay is based on the ability of macrophages to generate a strong inflammatory response when stimulated with antigens. Mouse immortalized macrophages (RAW 264.7 cell line) are stimulated by *E. coli* LPS and exposed to the test material for 24 hours. At the end of the incubation period, NO production is evaluated indirectly by measuring the accumulation of nitrite/nitrate, the stable end-products of NO oxidation, in the culture medium using a spectrophotometric method based on the Griess reaction [1,7].

Mouse macrophages (RAW 264.7, Sigma-Aldrich, N° P6110401, Lot. 09I006), low passage number (<50) were grown in DMEM with stable L-glutamine (Dulbecco's Minimum Essential Medium, PAN BIOTECH.) supplemented with Penicillin 100 IU/ml and streptomycin 100 µg/mL(PAN BIOTECH,), and 10% of inactivated calf serum (PAN BIOTECH,), pH 7.2, freshly prepared, stored no longer than 3 weeks. The test materials were diluted into dimethylsulfoxide (DMSO, Sigma-Aldrich), DMSO (0.5%) was used as a negative control and dexamethasone (Sigma-Aldrich) 1 – 5 – 10 – 50 – 100 µM was used as positive control. Cells were seeded into 96-well tissue culture plates at the concentration of 1.10^5 cells/mL (200 µL/well) for 24 hours at 37°C (5% CO_2). At the end of the incubation period the culture medium was replaced by 200 µL of medium containing the appropriate concentrations of the test materials, and cells were incubated at 37°C (5% CO_2) for one hour. At the end of the incubation period, pro-inflammatory LPS from *E.c*oli was added to cell cultures (1µg/mL). Then cells were incubated at 37°C (5% CO_2) for 24 hours. NO release was measured in the culture supernatant by the Griess reaction. 100 µL of the supernatants were transferred into the wells of a 96-well tissue culture plate, and 100 µL of the Griess modified reagent (SIGMA-ALDRICH) were added in each well. After a 15 min period at room temperature, the Optical Density (OD) of each well was read at 540 nm by a fluorescence-luminescence reader Infinite M200 Pro (TECAN). The results obtained for wells treated with the test material were compared to those of untreated control wells (DMSO, 100% viability) and converted to percentage values. In parallel to the assessment of NO release, cell viability was measured to validate the assay. The WST-1 vital dye reagent was used to measure cell mitochondrial respiration. For this purpose, the culture medium was decanted and 100µl of WST-1 reagent (1/10 dilution) were added in each well. After a 30-min incubation period at 37°C (5% CO2), the Optical Density (OD) of each well was read at 450 nm by a fluorescence-luminescence reader Infinite M200 Pro (TECAN). The results obtained for wells treated with the test material were compared to those of untreated control wells (DMSO, 100% viability) and converted to percentage values. Inhibition of NO release and inhibition of cell viability were expressed as percentages as compared to the negative controls:

$$\text{Percentage of NO release} = \frac{100 \times (\text{OD of test well} - \text{OD of blank})}{\text{OD of DMSO control} - \text{OD oof blank}}$$

$$\text{Percentage of Cell viabilty} = \frac{100 \times (\text{OD of test well} - \text{OD of blank})}{\text{OD of DMSO control} - \text{OD oof blank}}$$

The concentrations of the test material causing respectively a 50% decrease of NO release ($IC_{50\text{-NO release}}$) and a 50% decrease of cell viability ($IC_{50\text{-cell viability}}$) were calculated using software Tablecurve Version 2.0. The anti-inflammatory ratio corresponded to the ratio between the anti-inflammatory activity and the toxicity. It was expressed as follows:

$$\text{Anti-inflammatory ratio} = IC_{50\text{-cell viability}} / IC_{50\text{-NO release}}$$

Cytotoxicity investigation on Hep-G2 cell line

Cytotoxicity of the synthesized sulfonamide-*β*-lactam hybrids was assessed on Hep-G2 cell line using standard MTT colorimetric assay according to Gholami et al [64,65]. Six concentrations from 1 µM to 200 µM of 12 sulfonamide-*β*-lactam hybrids were studied. HepG2 cell pellets were suspended in RPMI 1640 media containing 10% fetal bovine serum comprising 1×10^5 cells/mL. Then, aliquots of 100 µL of suspension was infused in 96-well cell culture plates to obtain 1×10^4 cells/well and incubated at 37 °C in the presence of humidified atmosphere of 5% CO2 and 95% air to allow the cells to adhere and reach roughly 80% confluence. After 24 h, 100 µL of RPMI medium containing different concentrations of each compounds were replaced with media in each well and the plates incubated at 37 °C in atmosphere of 5% CO2 and 95% air. After 24 or 48 h, the medium was discarded and the wells were washed twice for 3 min with 100 µL phosphate buffered saline (PBS). For staining the viable cells, 25 µL of MTT [3-(4,5-dimethylthiazol2-yl)-2,5-diphe-nyltetrazolium bromide] solution (Sigma-Aldrich Co., St. Louis, MO, USA) (4 mg/mL in media) was added to each well and incubated again for 3 h at 37 ° C. The reaction was stopped and the formazan dye was solubilized by adding 100 µL of dimethylsulfoxide (DMSO). To completely dissolve the formazan crystals, plate was shaken well and the optical absorption of each solution was read at 540 nm using a microplate spectrophotometer (PowerWave X52, BioTek Instruments Inc., US). The average value was calculated from three treated wells and the values for medium alone were subtracted. In this experiment, the wells containing culture medium were regarded as the negative control (0% viability) and wells containing untreated HepG2 cells were considered as the positive control (100%). The optical density (OD) values of all samples were then analyzed by

% cell viability = [OD (Cells + Sample) – OD (Sample)] / [OD (Cells) – OD (RPMI)] × 100

The cell viability of three wells containing the same sample was compared with the positive control. The concentration of the compounds exhibited 50% of cell viability for HepG2 cells (IC_{50}) was calculated by nonlinear regression analysis of the response-concentration (log) curve. Results are expressed as the mean ±

SD of three different experiments. All calculated IC_{50} values were performed using CurveExpertPro software 1.6.5.

All statistical analyses were done using SPSS IBM ver. 23. For statistical comparison of cytotoxic activity, the one-way analysis of variance combined with Tukey's multiple range post-test was performed. This experiment was repeated three times. A P value below 0.05 was considered as statistically significant.

In vitro essay of antibacterial activity

Both of the following microorganisms *Staphylococcus aureus*, *Escherichia coli* were suspended in freshly prepared Mueller-Hinton's broth (MHB) at a standard concentration of 0.5 McFarland and diluted with a 1:20 proportion by MHB. An aqueous suspension was prepared from each of synthesized compounds so that the range of concentration would contain 1 µM to 32 µM of compounds. A 96-well microplate consisting of 45 µL culture media, 45 µL of sample (at a descending concentration of compounds from 32 µM to 1 µM), and 10 µL of inoculated bacteria was applied for each microorganism. The first and last rows of the microplate were left empty to achieve a better optical contrast after plate reading. The prepared microplates were incubated for 24 hours at 37 C; then, the optical density was measured at 600 nm by a microplate reader (BioTek, PowerWave XS2). This procedure was repeated three times. A blank 96-well microplate consisting of 45 µL of culture media and 45 µL of the sample (as explained) was prepared. At the end, 10 µL of culture media was added to each well. The turbidity of each well in a sample microplate (a microplate with the concerned microorganism) was compared to an equivalent well in a blank microplate. Microorganism viability was calculated as follows:

$$\%\ \text{microorganism viability} = [OD_{(\text{bacteria + sample})} - OD_{(\text{Sample})}] / [OD_{(\text{bacteria})} - OD_{(\text{RPMI})}] \times 100$$

All antimicrobial studies were evaluated using IBM SPSS software. To determine the differences between the means of the results, the one-way ANOVA procedure and the post hoc Tukey test were performed. P value ≤ 0.05 was considered to be statistically significant. The experiment was repeated three times [66,67].

Computational details

In silico physicochemical parameters and ADME profiling calculations

The physicochemical properties and drug-likeness for the synthesized compounds were calculated using SwissADME online software. Therefore, all compounds were evaluated for its drug-like nature under Lipinski's rules of five [59,68] and Verber [69,70]. ADMET refers to pharmacokinetic properties that deal primarily with Absorption, Distribution, Metabolism, Excretion, and Toxicity of the compounds in the human body. ADMET analysis of the potent compounds **4b** and **4h** were determined using the pkCSM [60] and protox-II webserver [61].

Docking simulation method

Due to the existence of various 3D-structures for iNOS, docking validation was used to select a proper x-ray structure for docking simulation. Amongst all these complexes, 6 3D X-ray crystal structures of the inducible nitric oxide synthase (iNOS) were picked out from the Protein Data Bank (PDB) (http://www.rcsb.org) in order to find the starting model of iNOS. The retrieved PDB codes for iNOS were 1NSI, 2NSI, 3E7G, 3EJ8, 4CX7 and 4NOS. Self-docking validation test was done with retrieved PDB codes. For running the selfdock, the innate ligands were re-docked on their corresponding 3D structures and the best pose of docking was superimposed with the native conformation of the ligands at crystallographic state. Five pdb files of the receptors were selected based on root-mean-square deviation (RMSD) values as shown in **Table 6**. The compound structures were sketched, energy minimized and the three ligand molecules were saved in pdbqt format. To prepare protein for docking simulation, all co-crystallized ligands and water molecules were excluded and the missing hydrogens were added. Non-polar hydrogens were merged with their corresponding carbons and then the protein was converted into the required pdbqt format. All preparation was performed using Auto Dock Tools package (1.5.6) [71].

After that, cross-docking simulations were performed using bash scripting in linux operating system. Autodock Vina (1.1.2) was applied for docking within a box defined by the following parameters. The grid box with the size of $30\times 30 \times 30$ was set and the box was centered on co-crystallized ligand. The center of grid box was determined as [x = 18.30, y = 64.66, z = 27.33] for 1NSI, [x = 17.88, y = 65.42, z = 27.14] for 2NSI, [x = 57.07, y = 22.18, z = 79.72] for 3E7G, [x = 67.20, y = 15.75, z = 76.89] for 3EJ8 and [x = 9.74, y = 97.54, z = 10.64] for 4NOS. The exhaustiveness was set to 100 and the other docking parameters were determined as default. At the end of cross-docking simulations, the best docking poses were selected for further analysis of enzyme-inhibitor interactions.

Acknowledgments

The authors gratefully acknowledge support by the Shiraz University Research Council. This work was supported by Shiraz University Research Council (Grant No. 98-GR-SC-23).

Keywords: 2-Azetidinone, Cycloaddition reaction, Biological activity, *In silico,* ADMET.

References

[1] M. A. Cinelli, H. T. Do, G. P. Miley, R. B. Silverman, *Med. Res. Rev.* **2020**, *40*, 158–189.

[2] W. K. Alderton, C. E. Cooper, R. G. Knowles, *Biochem. J.* **2001**, *357*, 593–615.

[3] B. C. Kone, T. Kuncewicz, W. Zhang, Z.-Y. Yu, *Am. J. Physiol. Physiol.* **2003**, *285*, F178–F190.

[4] J. N. Sharma, A. Al-Omran, S. S. Parvathy, *Inflammopharmacology* **2007**, *15*, 252–259.

[5] J. MacMicking, Q. Xie, C. Nathan, *Annu. Rev. Immunol.* **1997**, *15*,

323–350.
[6] Y. Yang, T. Yu, Y. Lian, R. Ma, S. Yang, J. Y. Cho, *Expert Opin. Ther. Pat.* **2015**, *25*, 49–68.
[7] S. Naureckiene, W. Edris, S. K. Ajit, A. H. Katz, K. Sreekumar, K. E. Rogers, J. D. Kennedy, P. G. Jones, *J. Pharmacol. Toxicol. Methods* **2007**, *55*, 303–313.
[8] J. M. Hevel, M. A. Marletta, **1994**, pp. 250–258.
[9] A. A.-M. Abdel-Aziz, A. Angeli, A. S. El-Azab, M. E. A. Hammouda, M. A. El-Sherbeny, C. T. Supuran, *Bioorg. Chem.* **2019**, *84*, 260–268.
[10] S. M. Sondhi, R. Rani, P. P. Gupta, S. K. Agrawal, A. K. Saxena, *Mol. Divers.* **2009**, *13*, 357–366.
[11] V. Gorantla, R. Gundla, S. S. Jadav, S. R. Anugu, J. Chimakurthy, S. K. Nidasanametla, R. Korupolu, *New J. Chem.* **2017**, *41*, 13516–13532.
[12] H. Moreno-Díaz, R. Villalobos-Molina, R. Ortiz-Andrade, D. Díaz-Coutiño, J. L. Medina-Franco, S. P. Webster, M. Binnie, S. Estrada-Soto, M. Ibarra-Barajas, I. León-Rivera, G. Navarrete-Vázquez, *Bioorg. Med. Chem. Lett.* **2008**, *18*, 2871–2877.
[13] M. J. Naim, O. Alam, M. J. Alam, M. Q. Hassan, N. Siddiqui, V. G. M. Naidu, M. I. Alam, *Bioorg. Chem.* **2018**, *76*, 98–112.
[14] Y. Ding, K. L. Smith, C. V. N. S. Vara Prasad, B. Wang, *Lett. Org. Chem.* **2018**, *15*, DOI 10.2174/1570178614666171010162204.
[15] K. Szafrański, J. Sławiński, A. Kędzia, E. Kwapisz, *Molecules* **2017**, *22*, 1926.
[16] A. K. Rathi, R. Syed, H.-S. Shin, R. V. Patel, *Expert Opin. Ther. Pat.* **2016**, *26*, 777–797.
[17] Z.-S. Gu, A. Zhou, Y. Xiao, Q.-W. Zhang, J.-Q. Li, *Eur. J. Med. Chem.* **2018**, *144*, 701–715.
[18] M. Singh, H. R. Jadhav, A. Kumar, *Lett. Drug Des. Discov.* **2018**, *15*, 866–874.
[19] M. S. Jain, S. J. Surana, *Arab. J. Chem.* **2017**, *10*, S2032–S2039.
[20] S. Chander, P. Wang, P. Ashok, L.-M. Yang, Y.-T. Zheng, M. Sankaranarayanan, *Bioorg. Med. Chem. Lett.* **2017**, *27*, 61–65.
[21] S. Tahir, T. Mahmood, F. Dastgir, I. Haq, A. Waseem, U. Rashid, *Eur. J. Med. Chem.* **2019**, *166*, 224–231.
[22] N. Thamban Chandrika, S. K. Shrestha, H. X. Ngo, O. V. Tsodikov, K. C. Howard, S. Garneau-Tsodikova, *J. Med. Chem.* **2018**, *61*, 158–173.
[23] P. Leren, A. Helgeland, I. Holme, P. O. Foss, I. Hjermann, P. G. Lund-Larsen, *Lancet* **1980**, *316*, 4–6.
[24] H. U. Lehmann, P. Ghabussi, H. Hochrein, *Med. Welt* **1977**, *28*, 386–90.
[25] J. Buch, *Adv. Ther.* **2010**, *27*, 426–443.
[26] M. Taha, M. Irshad, S. Imran, S. Chigurupati, M. Selvaraj, F. Rahim, N. H. Ismail, F. Nawaz, K. M. Khan, *Eur. J. Med. Chem.* **2017**, *141*, 530–537.
[27] C. J. Bungard, P. D. Williams, J. Schulz, C. M. Wiscount, M. K. Holloway, H. M. Loughran, J. J. Manikowski, H.-P. Su, D. J. Bennett, L. Chang, X.-J. Chu, A. Crespo, M. P. Dwyer, K. Keertikar, G. J. Morriello, A. W. Stamford, S. T. Waddell, B. Zhong, B. Hu, T. Ji, T. L. Diamond, C. Bahnck-Teets, S. S. Carroll, J. F. Fay, X. Min, W. Morris, J. E. Ballard, M. D. Miller, J. A. McCauley, *ACS Med. Chem. Lett.* **2017**, *8*, 1292–1297.
[28] A. K. Ajeesh Kumar, K. B. Nair, Y. D. Bodke, G. Sambasivam, K. G. Bhat, *Monatshefte für Chemie - Chem. Mon.* **2016**, *147*, 2221–2234.
[29] J. N. Narendra Sharath Chandra, C. T. Sadashiva, C. V. Kavitha, K. S. Rangappa, *Bioorg. Med. Chem.* **2006**, *14*, 6621–6627.
[30] A. Bhatt, R. Kant, *Med. Chem. (Los. Angeles).* **2016**, *06*, DOI 10.4172/2161-0444.1000355.
[31] B. R. Rao, M. R. Katiki, K. Dileep, C. G. Kumar, G. N. Reddy, J. B. Nanubolu, M. S. R. Murty, *Lett. Org. Chem.* **2019**, *16*, 723–734.
[32] T. Sperka, J. Pitlik, P. Bagossi, J. Tözsér, *Bioorg. Med. Chem. Lett.* **2005**, *15*, 3086–3090.
[33] A. Jarrahpour, M. Aye, J. A. Rad, S. Yousefinejad, V. Sinou, C. Latour, J. M. Brunel, E. Turos, *J. Iran. Chem. Soc.* **2018**, *15*, 1311–1326.
[34] A. Jarrahpour, S. Rezaei, V. Sinou, C. Latour, J. M. Brunel, *Iran. J. Sci. Technol. Trans. A Sci.* **2017**, *41*, 337–342.
[35] N. B. Patel, M. D. Patel, *Med. Chem. Res.* **2017**, *26*, 1772–1783.
[36] N. Borazjani, A. Jarrahpour, J. A. Rad, M. Mohkam, M. Behzadi, Y. Ghasemi, S. Mirzaeinia, H. R. Karbalaei-Heidari, M. M. Ghanbari, G. Batta, E. Turos, *Med. Chem. Res.* **2019**, *28*, 329–339.
[37] M. Mohamadzadeh, M. Zarei, M. Vessal, *Bioorg. Chem.* **2020**, *95*, 103515.
[38] G. Cainelli, C. Angeloni, R. Cervellati, P. Galletti, D. Giacomini, S. Hrelia, R. Sinisi, *Chem. Biodivers.* **2008**, *5*, 811–829.
[39] Y. U. Cebeci, H. Bayrak, Y. Şirin, *Bioorg. Chem.* **2019**, *88*, 102928.
[40] N. Borazjani, S. Sepehri, M. Behzadi, A. Jarrahpour, J. A. Rad, M. Sasanipour, M. Mohkam, Y. Ghasemi, A. R. Akbarizadeh, C. Digiorgio, J. M. Brunel, M. M. Ghanbari, G. Batta, E. Turos, *Eur. J. Med. Chem.* **2019**, *179*, 389–403.
[41] R. Heiran, S. Sepehri, A. Jarrahpour, C. Digiorgio, H. Douafer, J. M. Brunel, A. Gholami, E. Riazimontazer, E. Turos, *Bioorg. Chem.* **2020**, *102*, 104091.
[42] M. Rashidi, M. R. Islami, S. Esmaeili-Mahani, *Tetrahedron* **2018**, *74*, 835–841.
[43] A. M. Malebari, L. M. Greene, S. M. Nathwani, D. Fayne, N. M. O'Boyle, S. Wang, B. Twamley, D. M. Zisterer, M. J. Meegan, *Eur. J. Med. Chem.* **2017**, *130*, 261–285.
[44] K. Tahlan, S. E. Jensen, *J. Antibiot. (Tokyo).* **2013**, *66*, 401–410.
[45] R. B. Sykes, D. P. Bonner, K. Bush, N. H. Georgopapadakou, J. S. Wells, *J. Antimicrob. Chemother.* **1981**, *8*, 1–16.
[46] K. R. Lindner, D. P. Bonner, W. H. Koster, in *Kirk-Othmer Encycl. Chem. Technol.*, John Wiley & Sons, Inc., Hoboken, NJ, USA, **2000**.
[47] H. S. Patel, H. J. Mistry, *Phosphorus. Sulfur. Silicon Relat. Elem.* **2004**, *179*, 1085–1093.
[48] S. G. Shingade, S. B. Bari, *Med. Chem. Res.* **2013**, *22*, 699–706.
[49] R. Khanam, R. Kumar, I. I. Hejazi, S. Shahabuddin, R. Meena, V. Jayant, P. Kumar, A. R. Bhat, F. Athar, *Apoptosis* **2018**, *23*, 113–131.
[50] A. Mermer, H. Bayrak, Y. Şirin, M. Emirik, N. Demirbaş, *J. Mol. Struct.* **2019**, *1189*, 279–287.
[51] X. Qian, B. Zheng, B. Burke, M. T. Saindane, D. R. Kronenthal, *J. Org. Chem.* **2002**, *67*, 3595–3600.
[52] J. C. Sutton, S. A. Bolton, K. S. Hartl, M.-H. Huang, G. Jacobs, W. Meng, M. L. Ogletree, Z. Pi, W. A. Schumacher, S. M. Seiler, W. A. Slusarchyk, U. Treuner, R. Zahler, G. Zhao, G. S. Bisacchi, *Bioorg. Med. Chem. Lett.* **2002**, *12*, 3229–3233.
[53] G. S. Bisacchi, W. A. Slusarchyk, S. A. Bolton, K. S. Hartl, G. Jacobs, A. Mathur, W. Meng, M. L. Ogletree, Z. Pi, J. C. Sutton, U. Treuner, R. Zahler, G. Zhao, S. M. Seiler, *Bioorg. Med. Chem. Lett.* **2004**, *14*, 2227–2231.
[54] J. C. Sutton, S. A. Bolton, M. E. Davis, K. S. Hartl, B. Jacobson, A. Mathur, M. L. Ogletree, W. A. Slusarchyk, R. Zahler, S. M. Seiler, G. S. Bisacchi, *Bioorg. Med. Chem. Lett.* **2004**, *14*, 2233–2239.
[55] N. Borazjani, M. Behzadi, M. Dadkhah Aseman, A. Jarrahpour, J. A. Rad, S. Kianpour, A. Iraji, S. M. Nabavizadeh, M. M. Ghanbari, G. Batta, E. Turos, *Med. Chem. Res.* **2020**, *29*, 1355–1375.
[56] M. Alborz, A. Jarrahpour, R. Pournejati, H. R. Karbalaei-Heidari, V. Sinou, C. Latour, J. M. Brunel, H. Sharghi, M. Aberi, E. Turos, L. Wojtas, *Eur. J. Med. Chem.* **2018**, *143*, 283–291.
[57] M. Bashiri, A. Jarrahpour, B. Rastegari, A. Iraji, C. Irajie, Z. Amirghofran, S. Malek-Hosseini, M. Motamedifar, M. Haddadi, K. Zomorodian, Z. Zareshahrabadi, E. Turos, *Monatshefte für Chemie - Chem. Mon.* **2020**, *151*, 821–835.
[58] A. Jarrahpour, R. Heiran, V. Sinou, C. Latour, L. D. Bouktab, J. M. Brunel, J. Sheikh, T. B. Hadda, *Iran. J. Pharm. Res.* **2019**, *18*.
[59] C. A. Lipinski, F. Lombardo, B. W. Dominy, P. J. Feeney, *Adv. Drug Deliv. Rev.* **1997**, *23*, 3–25.
[60] D. E. V. Pires, T. L. Blundell, D. B. Ascher, *J. Med. Chem.* **2015**, *58*, 4066–4072.
[61] P. Banerjee, A. O. Eckert, A. K. Schrey, R. Preissner, *Nucleic Acids Res.* **2018**, *46*, W257–W263.
[62] "http://tox.charite.de/protox_II/index.php?site=compound_input/," can be found under http://tox.charite.de/protox_II/index.php?site=compound_input/, **n.d.**
[63] Y.-H. Hwang, M.-S. Kim, I.-B. Song, J.-H. Lim, B.-K. Park, H.-I. Yun, *Biotechnol. Lett.* **2009**, *31*, 789–795.
[64] L. Zamani, S. Khabnadideh, K. Zomorodian, A. Sakhteman, A. Gholami, Z. Rezaei, A. Mehdipoor, M. E. Dehkordi, R. Mortazavi, S. Ghafari, *Polycycl. Aromat. Compd.* **2019**, 1–21.
[65] A. Gholami, S. Rasoul-amini, A. Ebrahiminezhad, S. H. Seradj, Y. Ghasemi, *J. Nanomater.* **2015**, *2015*, 1–9.
[66] A. Gholami, F. Mohammadi, Y. Ghasemi, N. Omidifar, A. Ebrahiminezhad, *IET Nanobiotechnology* **2020**, *14*, 155–160.
[67] S. Zargarnezhad, A. Gholami, M. Khoshneviszadeh, S. N. Abootalebi, Y. Ghasemi, *J. Nanomater.* **2020**, *2020*, 1–9.
[68] P. Leeson, *Nature* **2012**, *481*, 455–456.
[69] D. F. Veber, S. R. Johnson, H.-Y. Cheng, B. R. Smith, K. W. Ward, K. D. Kopple, *J. Med. Chem.* **2002**, *45*, 2615–2623.
[70] C. Rao, R. P. Yejella, R. Rehman, S. H. Basha, *Bioinformation* **2015**, *11*, 322–329.
[71] E. Riazimontazer, H. Sadeghpour, H. Nadri, A. Sakhteman, T. Tüylü Küçükkılınç, R. Miri, N. Edraki, *Bioorg. Chem.* **2019**, *89*, 103006.

Entry for the Table of Contents

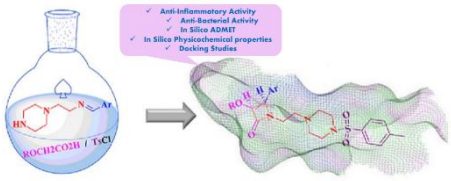

- Some newly sulfonamide-*β*-lactam hybrids incorporating the piperazine moiety were synthesized.
- Two derivatives demonstrated a similar therapeutic ratio to dexamethasone.
- Four derivatives showed good antibacterial activity against either E. coli and S. aureus in comparison with ampicillin as a standard.
- All compounds showed low cytotoxicity towards HepG2 cell line.
- Molecular docking analysis supported the *in vitro* results.